RSC Advances

PAPER

View Article Online
View Journal | View Issue

Cite this: *RSC Adv.*, 2022, **12**, 21191

Electronic effects on the mechanism of the NAD^+ coenzyme reduction catalysed by a non-organometallic ruthenium(II) polypyridyl amine complex in the presence of formate †

Marta Chrzanowska, [a] Anna Katafias, [a] Rudi van Eldik *[ab] and Jeanet Conradie *[cd]

In the present study, electronic effects on the mechanism of the NAD^+ coenzyme reduction in the presence of formate, catalysed by a non-organometallic ruthenium(II) polypyridyl amine complex, were investigated. The $[Ru^{II}(terpy)(ampy)Cl]Cl$ (terpy = 2,2′:6′,2″-terpyridine, ampy = 2-(aminomethyl)pyridine) complex was employed as the catalyst. The reactions were studied in a water/ethanol mixture as a function of formate, catalyst, and NAD^+ concentrations at 37 °C. The overall process was found to be 11 to 18 times slower than for the corresponding ethylenediamine (en) complex as the result of π-back bonding effects of the ampy ligand. The mechanistic studies revealed a complete set of reactions that accounted for the overall catalytic cycle based on a formate-induced hydride transfer reaction to form the reduced coenzyme, NADH. The geometries of the ruthenium(II)-ampy complexes involved in the catalytic cycle and free energy changes for the main steps were predicted by DFT calculations. Similar calculations were also performed for the analogues ruthenium(II)-en and ruthenium(II)-bipy complexes (bipy = 2,2′-bipyridine). The DFT calculated energies show that both the solvent-formato exchange and the formato-hydrido conversion reactions have negative (favourable) energies to proceed spontaneously. The reactions involving the en complex have the more negative (favourable) reaction energies, followed by the ampy complex, in agreement with faster reactions for en complexes and slower reactions for bipy complexes than for ampy complexes.

Received 23rd March 2022
Accepted 12th July 2022

DOI: 10.1039/d2ra01890j

rsc.li/rsc-advances

Introduction

It is well known that reducing pyridinium salts to dihydropyridine compounds is one of the metabolism-sustaining processes.[1,2] Eqn (1) presents one of such processes in all living cells.

$$NAD^+ + 2e^- + H_{aq}^+ \rightleftharpoons NADH \quad (1)$$

NAD^+ and NADH are the oxidised and reduced forms of nicotinamide adenine dinucleotide (NAD) coenzyme, respectively. The reaction outlined in eqn (1) involves the transfer of two electrons and one proton (PCET), which equals the transfer of a hydride ion, H^-. The process is fully reversible, and the NAD^+/NADH couple is a crucial biological electron/hydride transporter.[2,3] Therefore, NAD is fundamental for maintaining the optimal redox state of cells for their life and proper functioning. Loss of the redox balance (called redox stress) in favour of the reducing equivalents (reductive stress) or the reactive oxygen species (oxidative stress) results in cell damage or death, leading to various disorders of living organisms.[4] On the other hand, redox stress could be beneficial in treating many diseases, especially cancer.[5–8] The relationship between the redox (oxidative/reductive) stress and the pathogenic state of cells and modification of cellular redox balance as a novel approach to targeted therapeutic strategies are the subjects of many publications.[9–16]

An essential contribution to the development of redox-based therapy was made recently by Sadler and co-workers, who applied organometallic complexes to regulate the cellular redox state. It turned out that Ru(II) complexes with metal–carbon bonds alter the $[NAD^+]/[NADH]$ ratio using formate as a hydride source. Under such conditions, the balance between NAD^+ and NADH tilts towards the reduced form of the NAD coenzyme and

[a]*Faculty of Chemistry, Nicolaus Copernicus University in Toruń, Gagarina 7, 87-100 Toruń, Poland. E-mail: rudi.vaneldik@fau.de*

[b]*Department of Chemistry and Pharmacy, University of Erlangen-Nuremberg, Egerlandstr. 1, 91058 Erlangen, Germany*

[c]*Faculty of Natural and Agricultural Sciences, University of the Free State, Bloemfontein 9300, Republic of South Africa. E-mail: ConradJ@ufs.ac.za*

[d]*Department of Chemistry, UiT – The Arctic University of Norway, N-9037 Tromsø, Norway*

† Electronic supplementary information (ESI) available. See https://doi.org/10.1039/d2ra01890j

leads to reductive stress.[17–23] Being intrigued by the results of Sadler and co-workers, we successfully applied a non-organometallic $[Ru^{II}(terpy)(en)(H_2O/EtOH)]^{2+}$ complex (terpy = 2,2′:6′,2″-terpyridine, en = ethylenediamine) as a potential catalyst for the reduction of NAD^+ to NADH in the presence of formate.[24] Thus, the ability to catalyse the region-selective transfer of a hydride ion to NAD^+ is not a unique property of organometallic ruthenium(II) species, and similar effects can be reached in the presence of non-organometallic ruthenium(II) polypyridyl complexes. Based on kinetic and spectroscopic studies, we proposed the mechanism of the catalytic cycle for the reduction of NAD^+ to NADH in the presence of $[Ru^{II}(terpy)(en)(H_2O/EtOH)]^{2+}$ and formate in water/ethanol (1 : 9, v/v) solution.[24]

Recently, we reported results of our studies on tuning the reactivity of a series of analogues of the en complex mentioned above, of general formula $[Ru^{II}(terpy)(N\hat{}N)X]^{+/2+}$ (N^N = bidentate ligand, X = Cl^- or H_2O). We concluded that the rate of displacing a monodentate ligand, the first step of the proposed mechanism of the catalytic NAD^+–NADH conversion, depends on the electronic and steric effects provided by bidentate ligands.[25–28] Based on these studies, we expect that the catalytic efficiency will depend markedly on the nature of the coordinated bidentate ligand. The same effect was also observed for organometallic complexes studied by Sadler *et al.*[17,18,21] Therefore, we extended our work to the $[Ru^{II}(terpy)(ampy)Cl]Cl$ (ampy = 2-(aminomethyl)pyridine) and $[Ru^{II}(terpy)(bipy)Cl]Cl\cdot 2H_2O$ (bipy = 2,2′-bipyridine) complexes. These complexes are by one or two orders of magnitude less labile than the en analogue, for the aquation and water substitution reactions by chloride and thiourea at 25 °C, respectively.[28]

Experimental

Chemicals

All chemicals were of analytical reagent grade and used without further purification. $RuCl_3\cdot xH_2O$ was purchased from Abcam. 2-(Aminomethyl)pyridine, 2,2′:6′,2″-terpyridine, 2,2′-bipyridine, lithium chloride, methanol-d_4, deuterium oxide, sodium formate-d, β-nicotinamide adenine dinucleotide sodium salt, and MES sodium salt, were obtained from Merck. Sodium formate, sodium tetrahydroborate, and solvents were purchased from Avantor Performance Materials Poland SA. Deionized water was obtained from a Millipore Milli-Q water reagent system (Millipore, Bedford, MA, USA).

Synthesis of the complex

The $[Ru(terpy)(ampy)Cl]Cl$ and $[Ru(terpy)(bipy)Cl]Cl\cdot 2H_2O$ were synthesised according to procedures described earlier.[25,26] The complexes were fully characterised both in the solid-state and in solution, as reported before.[25,26] Solutions of $[Ru(terpy)(ampy)(H_2O)]^{2+}$ and $[Ru(terpy)(bipy)(H_2O)]^{2+}$ were prepared by spontaneous aquation of the parent chlorido complexes (*ca.* 2 h and 11 h, respectively) at room temperature. Solutions were prepared at least a day before the measurements.

Instrumentation

UV-Vis spectral analyses and kinetic studies were carried out using a conventional spectrophotometer Shimadzu UV-1601 PC and Shimadzu UV2600i with Peltier Temperature Controllers. Single wavelength kinetic data were processed with the EnzFiter software. ^1H NMR spectra were recorded on a Bruker Avance-700 NMR spectrometer in D_2O/CD_3OD (1 : 9, v/v) solution; chemical shifts were referenced to TMS.

Kinetic measurements

All Ru(II) aqua complex reactions were followed spectrophotometrically using a conventional method. The experiments were carried out in water/ethanol solutions (1 : 9, v/v, unless otherwise stated) in the presence of air. The temperature was kept constant at 36.8 ± 0.1 °C and controlled before and after each experiment. All measurements were repeated at least twice. The anation reaction, initiated by adding small aliquots of an aqueous solution of the aqua complex to the thermostated formate solution, was monitored as an absorbance increase at 517 nm.

Overall spectral changes accompanying the examined catalytic process were recorded within the 300–800 nm wavelength range. Reactions were initiated by adding small aliquots of a thermostated aqueous sodium formate solution to a thermostated water/ethanol solution of NAD^+ and the Ru(II) complex. Several experiments in solutions of varying water to ethanol volume ratios, namely 3 : 7, 1 : 1 and 1 : 3, were conducted to investigate the effect of alcohol concentration on the rate of the catalytic process. Additional kinetic tests were performed in MES buffer solutions of pH 7.1.

NMR and UV-Vis studies

A large excess of solid $NaBH_4$ was added to a deaerated hot solution of $[Ru(terpy)(ampy)(H_2O)]^{2+}$ in D_2O/CD_3OD (1 : 9, v/v) to synthesise the $[Ru(terpy)(ampy)H]^+$ complex. The final concentrations of the reagents were as follows: 6.4×10^{-3} M Ru(II), 0.26 M $NaBH_4$. The mixture was refluxed and a ^1H-NMR spectrum was recorded approximately 10 min after the reaction was initiated. To register an electronic absorption spectrum, the solution prepared as described above was diluted by introducing a few drops of it into an argon purged water/ethanol solution (1 : 9, v/v) in a gas-tight spectrophotometric cell.

DFT method

The density functional theory study on the compounds was done on the molecules in the gas phase, with the Scalar relativistic ZORA (Zeroth Order Regular Approximation to the Dirac equation)[29–31] Hamiltonian, the OLYP GGA (Generalized Gradient Approximation)[32,33] functional using Grimme's D3 dispersion correction[34] and ZORA TZ2P all-electron relativistic basis sets, all as implemented in the ADF program system.[35,36] Frequency analyses were done on all complexes to verify minima.

Results and discussion

Preliminary observations

***In situ* formation of [Ru(terpy)(ampy)H]$^+$.** Our previous work showed that the most critical step in reducing NAD^+ to NADH catalysed by a Ru(II) polypyridyl complex is forming a hydrido species.[24] Therefore, it was necessary to check the *in situ* generation of the hydride complex in the reaction of the $[Ru(terpy)(ampy)(H_2O/EtOH)]^{2+}$ complex with sodium borohydride, which was observed in the presence of the $[Ru(terpy)(en)(H_2O/EtOH)]^{2+}$ complex. The formation of $[Ru(terpy)(ampy)H]^+$ in the reaction with $NaBH_4$ is accompanied by an increase in absorbance intensity with a shift of the absorbance maxima from 535 to 520 nm and 380 to 394 nm (Fig. 1). A larger excess of sodium borohydride is required to produce the ampy-hydrido complex than its en analogue. In contrast to the previous study, the reaction was carried out at 37 °C (instead of 25 °C), which is in line with the differences in reactivity caused by various electronic and steric properties of the en and ampy ligands.[25–28] The conversion of the starting into the hydrido complex, which is stable under such conditions, is a straightforward process, demonstrated by isosbestic points at 371, 456, 545, and 568 nm.

^{1}H-NMR spectra were recorded to confirm the *in situ* formation of the hydrido complex using a much higher concentration of the complex and a larger excess of borohydride (selected conditions for the NMR experiment). A signal characteristic of the hydrido complex was observed at −27.59 ppm. Additional confirmation for the formation of the hydrido complex was obtained from a comparison of the UV-Vis spectrum of a diluted sample used in the NMR experiment with the last spectrum shown in Fig. 1 (see Fig. 2).

Since the $[Ru(terpy)(ampy)H]^+$ complex is stable under the conditions described above, CO_2(g) was passed through its solution to convert it into the corresponding formato complex. The observed shift of the absorption maxima towards shorter wavelengths (hypsochromic effect) is characteristic of the substitution of a hydride ion by formate, and proves the formation of the $[Ru(terpy)(ampy)(HCOO)]^+$ complex (Fig. 3). This experiment shows that it is possible to obtain the formato complex as described before for the corresponding en and bipy complexes.[24,37]

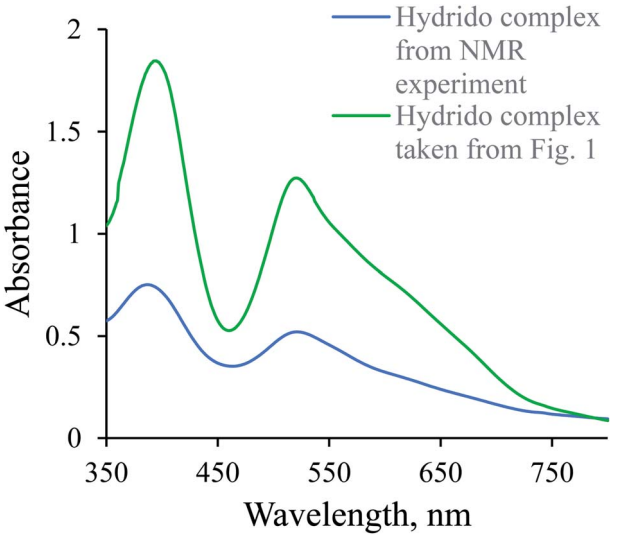

Fig. 2 UV-Vis spectra of $[Ru(terpy)(ampy)H]^+$ in water/ethanol (1 : 9, v/v) solution.

Blank experiments. Preliminary studies were performed to check that: (1) the ethanol present in the reaction mixture is not a hydride donor; (2) the hydride transfer reaction does not occur without the Ru(II) complex being present. For this purpose, two blank tests were performed. UV-Vis spectroscopy was used to monitor spectral changes for the reaction between NAD^+ and the $[Ru^{II}(terpy)(ampy)(H_2O/EtOH)]^{2+}$ complex in the absence of formate (Fig. 4a), and between NAD^+ and formate without the participation of the Ru(II) complex (Fig. 4b). Both experiments carried out in water/ethanol solution (1/9, v/v) showed no absorbance increase at 340 nm, characteristic of NADH formation. It means that the presence of both the $[Ru^{II}(terpy)(ampy)(H_2O/EtOH)]^{2+}$ complex and formate are

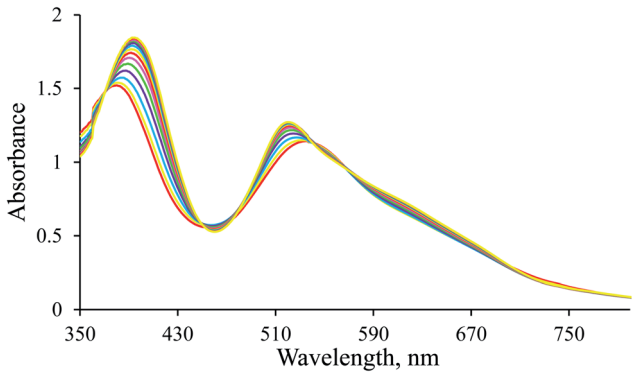

Fig. 1 Spectral changes observed for the formation of the $[Ru(terpy)(ampy)H]^+$ complex in water/ethanol (1 : 9, v/v) solution. Experimental conditions: $[Ru(II)] = 9.6 \times 10^{-2}$ mM, $[NaBH_4] = 7.8$ mM, argon atmosphere, $T = 37$ °C, $l = 1$ cm; spectra recorded every 200 s.

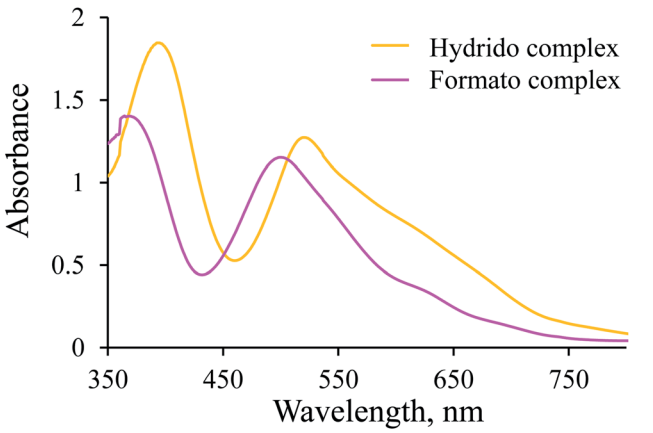

Fig. 3 Comparison of spectra of $[Ru(terpy)(ampy)H]^+$ and $[Ru(terpy)(ampy)(HCOO)]^+$ obtained during the reaction of the former one with CO_2(g) in water/ethanol (1 : 9, v/v) solution. Experimental conditions: $[Ru(II)] = 9.6 \times 10^{-2}$ mM, $T = 37$ °C, $l = 1$ cm.

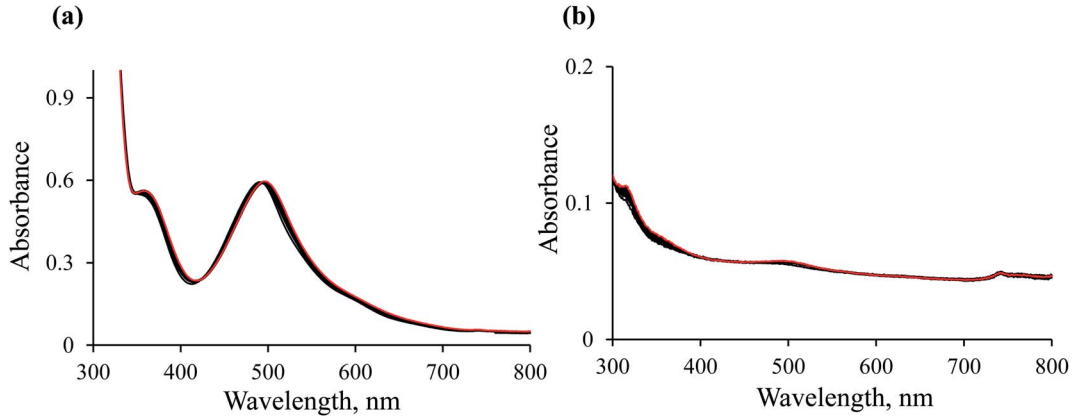

Fig. 4 Spectral changes observed during the reaction of 0.31 mM NAD^+ with 5.3×10^{-2} mM $[Ru(terpy)(ampy)(H_2O/EtOH)]^{2+}$ (a) and 0.31 mM NAD^+ with 29 mM formate (b) in water/ethanol (1 : 9, v/v) solution at $T = 36.8$ °C; spectra recorded every 60 min (black colour) and next day (red colour).

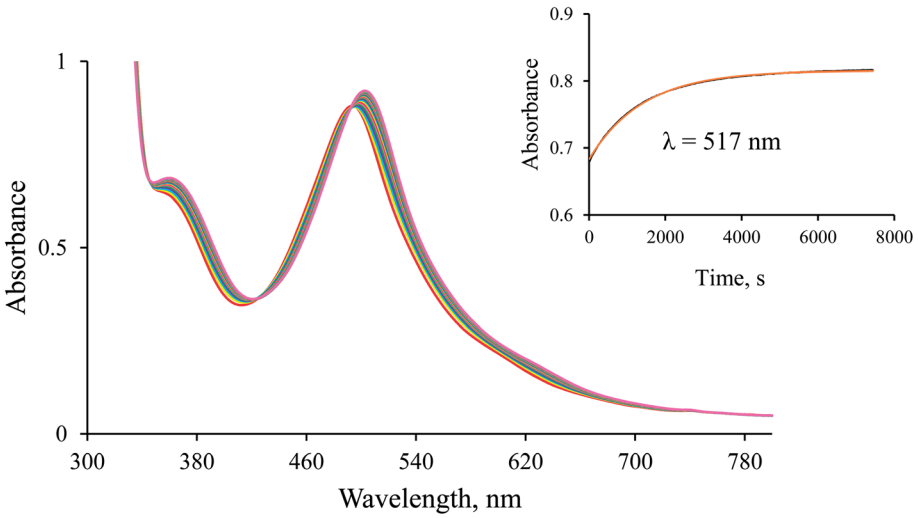

Fig. 5 Spectral changes observed during the anation of $[Ru^{II}(terpy)(ampy)(H_2O/EtOH)]^{2+}$ by formate in water/ethanol (1 : 9, v/v) solution. Experimental conditions: [Ru(II)] = 0.106 mM, $[HCOO^-] = 1.12$ mM, $T = 36.8$ °C; spectra recorded every 250 s. Inset: kinetic trace (black) along with a fit to a single exponential function (red).

required to induce the reduction of NAD^+ to NADH, and ethanol does not serve as a hydride donor.

Reaction of the Ru(II) complex with formate. To gain further mechanistic insight into the catalytic reduction of NAD^+, we studied the substitution reaction of $[Ru(terpy)(ampy)(H_2O/EtOH)]^{2+}$ by formate in H_2O/EtOH (1 : 9, v/v solution). The spectral changes accompanying the reaction are reported in Fig. 5. Kinetic traces recorded under pseudo-first-order conditions appeared to be single exponential, as demonstrated in the given inset.

The non-linear dependence of the pseudo-first-order rate constant (k_{obs}) on the formate concentration presented in Fig. 6 reveals the reversibility of the examined process, indicated by the significant intercept of the plot.

The kinetics of the formation of the formato complex can be accounted for in terms of a rate-determining ligand exchange

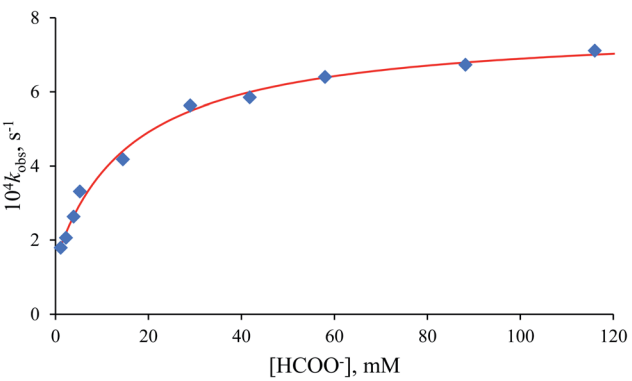

Fig. 6 Dependence of k_{obs} on $[HCOO^-]$ for the anation of $[Ru^{II}(terpy)(ampy)(H_2O/EtOH)]^{2+}$ by $HCOO^-$. Experimental conditions: [Ru(II)] = 0.106 mM, $T = 36.8$ °C, in water/ethanol (1 : 9, v/v) solution.

process (k_1 and k_{-1}), preceded by a rapid ion-pair formation step (Q_1) as outlined in eqn (2).

$$[Ru^{II}(terpy)(ampy)(H_2O/EtOH)]^{2+} + HCOO^- \rightleftharpoons \{[Ru^{II}(terpy)(ampy)(H_2O/EtOH)]^{2+} \cdot HCOO^-\} \quad Q_1$$
$$\Downarrow$$
$$[Ru^{II}(terpy)(ampy)(HCOO)]^{+} + H_2O/EtOH \quad k_1, k_{-1} \qquad (2)$$

The rate expression derived for reactions (2) is given in eqn (3),

$$k_{obs} = k_{-1} + \left(\frac{k_1 Q_1 [HCOO^-]}{1 + Q_1 [HCOO^-]}\right) \qquad (3)$$

where the overall equilibrium constant K is expressed by eqn (4):

$$K = \frac{k_1 Q_1}{k_{-1}} \qquad (4)$$

The obtained results demonstrate that the substitution reaction of $[Ru^{II}(terpy)(ampy)(H_2O/EtOH)]^{2+}$ with formate takes 6.5 h and 1.5 h at the lowest and highest formate concentration, respectively. It shows that the examined ampy complex reacts 11–18 times slower than its analogue $[Ru^{II}(terpy)(en)(H_2O/EtOH)]^{2+}$. This is in good agreement with detailed studies on the substitution behaviour of both complexes in an aqueous solution and is essential for revealing the mechanism of the catalytic process.[25,26,28]

The k_1/k_{-1} ratio found for the ampy complex is higher than that of the en analogue, favouring the formation of the formato complex. Values of the ion-pair formation constant Q_1 are similar for both complexes. In this way, the value of the overall equilibrium constant K for the ampy complex is much higher than for the en complex (Table 1). As a consequence, 24% of the Ru(II)-ampy complex and only 5% of the Ru(II)-en complex exist in the formato form in solution of the lowest formate concentration (*ca.* 1 mM), whereas in the case of the highest formate concentration (*ca.* 120 mM), 97% of $[Ru^{II}(terpy)(ampy)(H_2O/EtOH)]^{2+}$ and 87% of $[Ru^{II}(terpy)(en)(H_2O/EtOH)]^{2+}$ are converted into the formato complexes.

Kinetic data for the reaction of the Ru(II) complex with formate as a source of hydride for the conversion of NAD^+ to NADH. Subsequently, we checked the influence of the formate concentration on the kinetics of the reduction of NAD^+ to NADH. The observed spectral changes along with the development of a distinct peak at 340 nm support the formation of NADH *via* reduction of NAD^+ by $[Ru^{II}(terpy)(ampy)(H_2O/EtOH)]^{2+}$ in the presence of formate under the specified conditions. Important to note is that this process occurs on a much longer time scale than the formation of the $[Ru^{II}(terpy)(ampy)(HCOO)]^+$ complex. Spectral changes for the reduction of NAD^+ at low and high formate concentrations are presented in Fig. 7. At the lower and higher formate concentrations, the formation of NADH takes *ca.* 45 h and *ca.* 20 h, respectively. As expected, different electronic properties of the 2-(aminomethyl)pyridine ligand compared to ethylenediamine, affect the overall conversion time of NAD^+. The time scale for these reactions is approximately two times longer for the ampy complex than for the en analogue. The kinetics of the overall process changes with increasing formate concentration from first-order to zero-order (see inset in Fig. 7).

In general, all kinetic data obtained at $[HCOO^-] \leq 1.35$ mM showed first-order behaviour (see Fig. 7a), and the observed rate constant was independent of the formate concentration, with an average value of $(9.7 \pm 0.1) \times 10^{-6}$ s^{-1} at [Ru(II)] = 5.3×10^{-2} mM and 36.8 °C. Mixed zero- and first-order behaviour was observed in the range of $[HCOO^-] = 1.65$–2.20 mM. At $[HCOO^-] \geq 7.20$ mM, typical zero-order kinetic profiles with characteristic 'dead-ends' were recorded (see Fig. 7b).

The collected kinetic data as a function of formate concentration are summarised in Table S1.† Values of the initial rate and zero-order rate constants calculated at low and high excess of formate, respectively, show a non-linear dependence on the formate concentration and pass through the origin within the error limits (Fig. 8).

Table 1 Summary of the rate and equilibrium constants for the anation of $[Ru^{II}(terpy)(N\text{^}N)(H_2O/EtOH)]^{2+}$ in water/ethanol (1 : 9, v/v) solution. Experimental conditions: [Ru(II)] = 10.6×10^{-2} mM, T = 36.8 °C

	Value	
Parameter	$[Ru^{II}(terpy)(ampy)(H_2O/EtOH)]^{2+}$	$[Ru^{II}(terpy)(en)(H_2O/EtOH)]^{2+}$
k_1, s^{-1}	$(6.3 \pm 0.2) \times 10^{-4}$	$(4.8 \pm 0.2) \times 10^{-3}$
Q_1, M^{-1}	61 ± 10	41 ± 7
k_1Q_1, M^{-1} s^{-1}	0.039 ± 0.006	0.20 ± 0.04
k_{-1}, s^{-1}	$(1.4 \pm 0.2) \times 10^{-4}$	$(3.4 \pm 0.1) \times 10^{-3}$
$K = k_1Q_1/k_{-1}$, M^{-1}	286 ± 1	59 ± 13

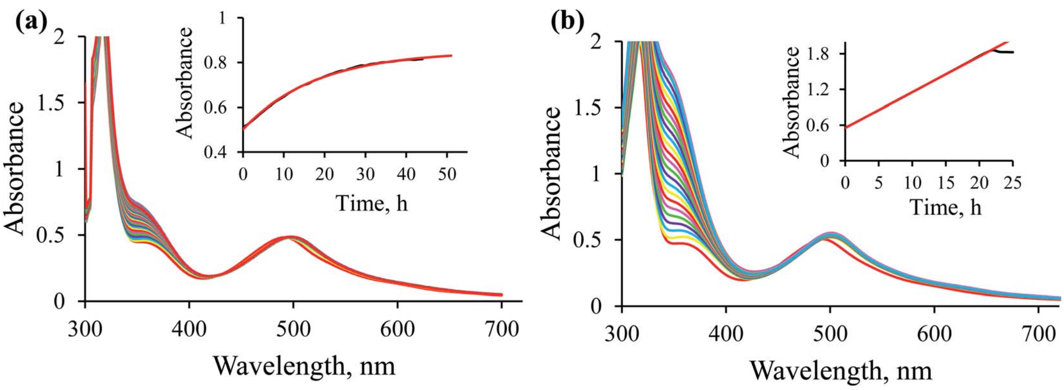

Fig. 7 Spectral changes observed during the reduction of NAD^+ to 1,4-NADH in the presence of formate in water/ethanol (1 : 9, v/v) solution. Experimental conditions: (a) $[HCOO^-] = 0.86$ mM, (b) $[HCOO^-] = 58$ mM; [Ru] = 0.053 mM, $[NAD^+] = 0.31$ mM, $T = 36.8$ °C; spectra recorded every 60 min. Insets: kinetic traces recorded at 340 nm (black) along with fits to a single exponential (a) and linear (b) functions.

This kind of dependence can be accounted for by the general reaction mechanism outlined in eqn (5) and (6):

$$[Ru^{II}(terpy)(ampy)(HCOO)]^+ + HCOO^- \underset{}{\overset{Q_2}{\rightleftharpoons}} \{[Ru^{II}(terpy)(ampy)(HCOO)]^+ \cdot HCOO^-\} \xrightarrow{k_2} [Ru^{II}(terpy)(ampy)H]^+ + HCOO^- + CO_2 \quad (5)$$

$$[Ru^{II}(terpy)(ampy)H]^+ + NAD^+ \underset{+H_2O}{\xrightarrow{fast}} [Ru^{II}(terpy)(ampy)(H_2O/EtOH)]^{2+} + NADH \quad (6)$$

A rapid and reversible formation (Q_2) of the ion-pair precursor $\{[Ru^{II}(terpy)(ampy)(HCOO)]^+ \cdot HCOO^-\}$ (eqn (5)) is followed by a rate-limiting generation (k_2) of the hydrido complex (eqn (5)), from which the hydride ion is transferred to NAD^+ in a fast subsequent reaction step (eqn (6)). Concomitantly, the starting $[Ru^{II}(terpy)(ampy)(H_2O/EtOH)]^{2+}$ complex is reformed. The experimental data in Fig. 8 were fitted to eqn (7):

$$r = \frac{d[NADH]}{dt} = \frac{k_2 Q_2 [HCOO^-]}{1 + Q_2 [HCOO^-]} \quad (7)$$

At low formate concentration, the rate law (7) simplifies to:

$$r = \frac{d[NADH]}{dt} = k_2 Q_2 [HCOO]^- \quad (8)$$

At high formate concentration, the rate law (7) simplifies to:

$$r = \frac{d[NADH]}{dt} = k_2 \quad (9)$$

The maximum rate of the overall process $k_2 = (9.4 \pm 0.1) \times 10^{-6}$ M h^{-1} and precursor ion-pair formation constant $Q_2 = 373 \pm 16$ M^{-1} at 36.8 °C. The initial slope of the plot in Fig. 8 is given

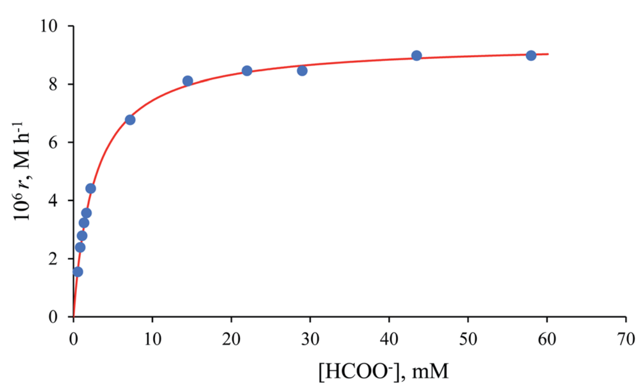

Fig. 8 Dependence of initial rate (for the first-order reactions followed at low formate concentrations) or zero-order rate constant (for the zero-order reactions at higher formate concentrations) on the $[HCOO^-]$ for the reduction of NAD^+ to 1,4-NADH in water/ethanol (1 : 9, v/v) solution. Experimental conditions: [Ru(II)] = 0.053 mM, $[NAD^+] = 0.31$ mM, $T = 36.8$ °C; r = initial rate or zero-order rate constant.

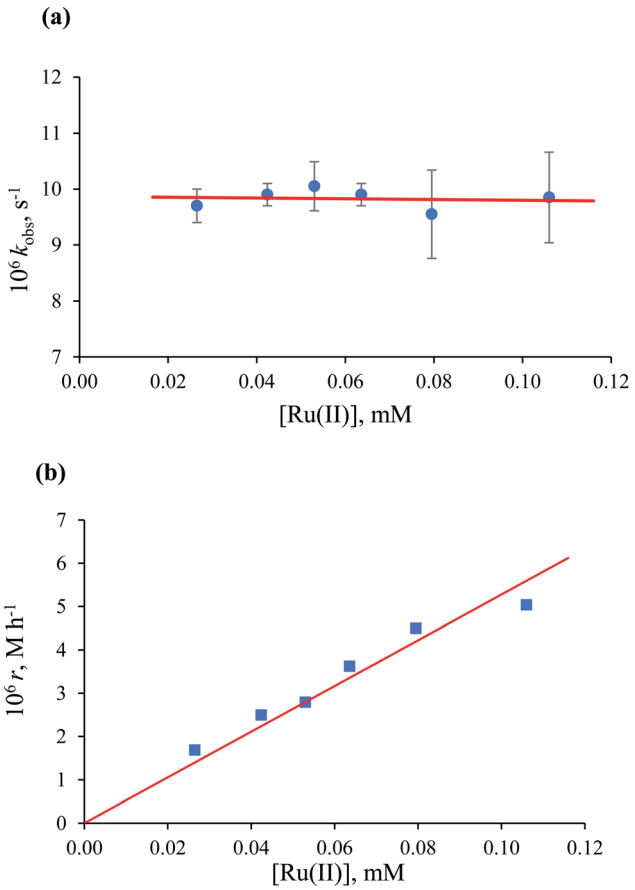

Fig. 9 Dependence of k_{obs} (a) and initial rate (b) on the [Ru(II)] for the catalysed reduction of NAD^+ to 1,4-NADH in H_2O/EtOH (1 : 9, v/v) solution. Experimental conditions: $[NAD^+] = 0.31$ mM, $[HCOO^-] = 1.1$ mM, $T = 36.8$ °C.

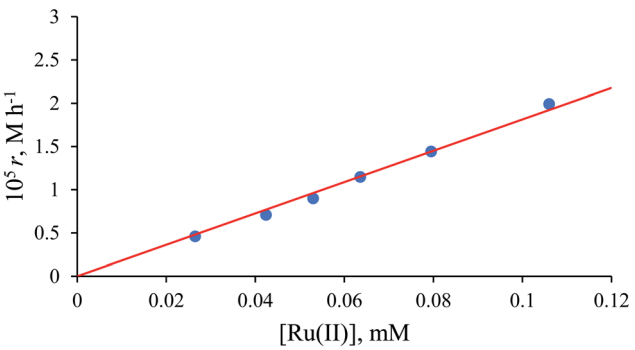

Fig. 10 Dependence of the initial rate on [Ru(II)] for the catalysed reduction of NAD^+ to 1,4-NADH in water/ethanol (1 : 9, v/v) solution. Experimental conditions: $[NAD^+] = 0.31$ mM, $[HCOO^-] = 43.5$ mM, $T = 36.8$ °C.

by $k_2Q_2 = (3.5 \pm 0.2) \times 10^{-3}$ h^{-1}, which is the first-order rate constant.

Kinetic data for NADH formation as a function of the Ru(II) concentration in the presence of formate. To obtain further information on the possible reduction of NAD^+ catalysed by $[Ru^{II}(terpy)(ampy)(H_2O/EtOH)]^{2+}$, we studied the reaction as a function of ruthenium(II) concentration. Experiments were carried out in the concentration range 0.027–0.106 mM at low and high formate concentrations, typical for the first-order and zero-order behaviour, respectively. The dependence of k_{obs} as a function of catalyst concentration shows that at low formate concentration, the first-order rate constant is independent of the Ru(II) concentration (Fig. 9a). This observation differs from that for the $[Ru^{II}(terpy)(en)(H_2O/EtOH)]^{2+}$ complex, for which a saturation effect was observed under the same experimental conditions. The result can be accounted for by the significantly higher value of the overall formation constant K for the $[Ru^{II}(terpy)(ampy)(HCOO)]^+$ complex, as compared to the

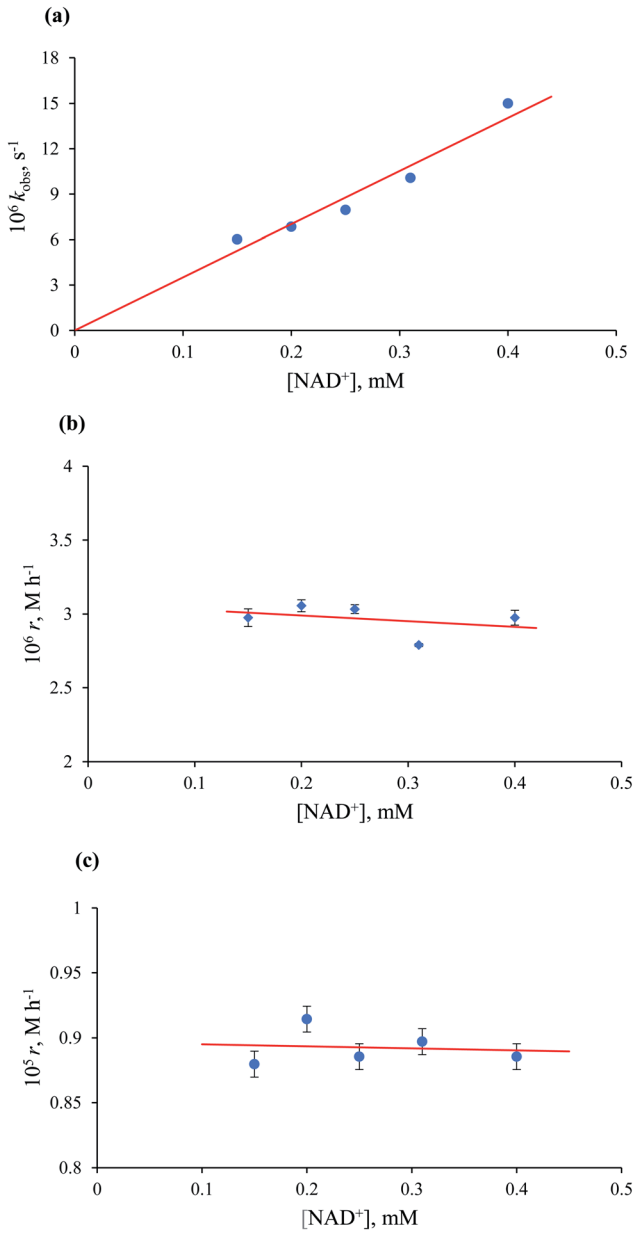

Fig. 11 Dependence of k_{obs} (a) and the initial rate (b) at 1.1 mM $HCOO^-$, and the initial rate (c) at 43.5 mM $HCOO^-$ on $[NAD^+]$ for the catalysed reduction of NAD^+ to 1,4-NADH in water/ethanol (1 : 9, v/v) solution. Experimental conditions: [Ru(II)] = 0.053 mM, $T = 36.8$ °C.

Table 2 Kinetic data for the catalytic reduction of NAD^+ to 1,4-NADH in water/ethanol solutions of varying composition

H_2O/EtOH, v/v	10^5 r, M h^{-1}	10^2 k_{obs}, h^{-1}	10^5 r^a, M h^{-1}
Ru-ampy[b]			
1 : 9	0.897 ± 0.001	—	—
3 : 7	0.883 ± 0.001	—	—
1 : 1	0.619 ± 0.001	—	—
3 : 1	—	0.79 ± 0.02	0.194 ± 0.001
Ru-en[c]			
1 : 9	1.97 ± 0.01	—	—
3 : 7	1.10 ± 0.01	—	—
1 : 1	—	2.2 ± 0.1	0.49 ± 0.06

[a] Initial rate. Experimental conditions: [Ru(II)] = 5.3×10^{-2} mM, [NAD^+] = 0.31 mM. [b] [$HCOO^-$] = 58 mM. [c] [$HCOO^-$] = 43.5 mM, T = 36.8 °C.

corresponding en complex, which suggests that the saturation effect has been reached under the selected conditions. The initial slope (r) increases linearly with the [Ru(II)] as indicated in Fig. 9b.

Values of the zero-order rate constant (r) obtained at high formate concentration show a linear dependence on the Ru(II) concentration (Fig. 10). All kinetic data are summarised in Table S2.†

Kinetic data for the formation of NADH as a function of NAD^+ concentration in the presence of formate. Experiments as a function of NAD^+ concentration were performed. The observed first-order and zero-order rate constants for the Ru(II)-en system reported before, were independent of the [NAD^+] at low and high formate concentrations, respectively. In contrast, the observed rate constant (k_{obs}) for the overall process catalysed by $[Ru^{II}(terpy)(ampy)(H_2O/EtOH)]^{2+}$ at low formate concentration, varied linearly with the NAD^+ concentration, as shown in Fig. 11a, whereas the initial rate (r) was found to be independent of the [NAD^+] (Fig. 11b, Table S3†). At high formate concentration, the zero-order rate constant was found to be independent of the NAD^+ concentration (Fig. 11c, Table S3†).

Kinetic isotope effect. Determining the kinetic isotope effect (KIE) in the presence of deuterated sodium formate helped elucidate the critical role of the hydride anion in the overall mechanism, *i.e.*, to check whether the formation of the hydride complex is the rate-limiting step of the process. A value of the rate constant for normal and deuterated sodium formate is $r_{HCOO^-} = (8.97 \pm 0.01) \times 10^{-6}$ M h^{-1} and $r_{DCOO^-} = (5.95 \pm 0.01) \times 10^{-6}$ M h^{-1}, respectively. The KIE causes a decrease in the rate of a chemical reaction when one of the atoms of the reactants is replaced with one of its heavier isotopes. For the reaction catalysed by $[Ru^{II}(terpy)(ampy)(H_2O/EtOH)]^{2+}$, the KIE equals 1.5. This value is smaller than the one determined for the $[Ru^{II}(terpy)(en)(H_2O/EtOH)]^{2+}$ (KIE = 2.4),[24] which is consistent with the literature data.[38] The decrease in the reaction rate due to the change of protium to deuterium indicates that the formation of the hydrido complex is the rate-limiting step of the overall process. It means that converting the formato to hydrido complex is the slowest step of the studied process.

Kinetic data as a function of the solvent composition. The solvent composition influence on the time scale and kinetics of the NAD^+-NADH conversion in the presence of the Ru-ampy complex was examined. The experiments were carried out at a high formate concentration. It was shown that on reducing the concentration of ethanol from 90 to 25%, the kinetics of the process change from zero- to first-order. Simultaneously its time scale increases from 24 h to 7 d, which is manifested by a decrease in the value of r by a factor of 5 (Table 2). An analogous kinetics change in the Ru-en complex presence takes place in 50% ethanol, and a decrease in the r value by a factor of 4 on going from 90 to 50% ethanol is observed. The slower reaction is due to the increase in the polarity of the solvent.

DFT studies. To shed light on the ruthenium reactants, products, and possible reaction intermediates for the formation of the hydrido species, density functional theory was applied. The geometries of the different species involved in the following two reactions (corresponding to reactions numbered (2) and (5) of this study for N^N = ampy),

$$[Ru^{II}(terpy)(N^N)(solvent)]^{2+} + HCOO^- \rightleftharpoons [Ru^{II}(terpy)(N^N)(HCOO^-)]^+ + solvent \quad (10)$$

and

$$[Ru^{II}(terpy)(N^N)(HCOO^-)]^+ + HCOO^- \rightleftharpoons [Ru^{II}(terpy)(N^N)H^+] + HCOO^- + CO_2 \quad (11)$$

for N^N = bipy, ampy and en, are shown in Fig. 12 (solvent = H_2O) and Fig. S2† (solvent = EtOH). The DFT calculated electronic and free energy changes for the DFT calculated reactions (10) and (11) are summarized in Table 3.

Table 3 OLYP/ZORA-TZ2P calculated electronic (ΔE) and free (ΔG) energies for the indicated reactions

DFT reaction	N^N	Solvent	Reactants	Products	ΔE (eV)	ΔG (eV)
(10)	Bipy	EtOH	$[Ru^{II}(terpy)(N^N)(solvent)]^{2+}$ + $HCOO^-$	$[Ru^{II}(terpy)(N^N)(HCOO)]^+$ + solvent	−6.54	−6.58
	Ampy				−6.62	−6.67
	en				−6.69	−6.70
	Bipy	H_2O			−6.91	−6.89
	Ampy				−7.00	−6.98
	en				−7.06	−7.01
(11)	Bipy		$[Ru^{II}(terpy)(N^N)(HCOO)]^+$ + $HCOO^-$	$[Ru^{II}(terpy)(N^N)H]^+$ + $HCOO^-$ + CO_2	0.02	−0.46
	Ampy				−0.08	−0.62
	en				−0.13	−0.71

The geometries of the $[Ru^{II}(terpy)(N^N)(solvent)]^{2+}$ reactant molecules of the DFT reaction (10) (reaction (2) for N^N = ampy) are distorted octahedral with the solvent molecules *trans* to the nitrogen of the N^N ligand. The N–Ru–N and N–Ru–O angles are lower than 90° as expected for a real octahedral molecule due to the strain of the tridentate terpy and bidentate N^N ligands. For the molecules containing the unsymmetrical ampy ligand, the solvent is coordinated *trans* to the amine nitrogen. The isomers of $[Ru^{II}(terpy)(ampy)(solvent)]^{2+}$ with the amine nitrogen *cis* to the solvent molecule are more than 0.1 eV higher (both electronic and free energy), for both solvents EtOH and H_2O and thus less likely. The obtained *trans* orientation also agrees with the fact that the $[Ru^{II}(terpy)(ampy)(solvent)]^{2+}$ molecules were obtained from [Ru(terpy)(ampy)Cl]Cl, where the Cl was experimentally shown to be *trans* to the amine nitrogen.[26] The DFT calculated geometries of $[Ru^{II}(terpy)(bipy)(H_2O)]^{2+}$ molecules and $[Ru^{II}(terpy)(en)(H_2O)]^{2+}$ molecules agree with the reported experimental solid-state structures (see ref. 25, 39 and 40 (bipy) and [ref. 25 and 41] (en)). Although experimental solid-state structures of $[Ru^{II}(terpy)(N^N)(EtOH)]^{2+}$ molecules could not be found in the literature, the DFT calculations indicate these molecules as stable, though the DFT reaction (10) for the molecules containing water, is slightly favoured compared to the reaction of the molecules with EtOH (lower electronic and free energy changes, Table 3).

When formate ($HCOO^-$) is added to $[Ru^{II}(terpy)(N^N)(solvent)]^{2+}$, hydrogen bonding between formate and the O atom of the solvent molecule occurs to produce a stable ion-pair reaction intermediate $\{[Ru^{II}(terpy)(N^N)(solvent)]^{2+}\cdot HCOO^-\}$. It is followed by the substitution of the coordinated solvent by formate to form a stable formate complex $[Ru^{II}(terpy)(N^N)(HCOO)]^+$, see the geometries in Fig. 12. The DFT calculated $[Ru^{II}(terpy)(N^N)(HCOO)]^+$ geometries agree with that of a reported experimental solid-state structure of $[Ru^{II}(terpy)(bipy)(HCOO)]^+$.[42]

The ion-pair formation step (reaction (2)) is much faster, with a more favourable free energy change of *ca.* −7 eV (*e.g.*, −6.91 eV for N^N = ampy and solvent = H_2O) than the slower substitution step (reaction (2)) with a much smaller free energy change of *ca.* −0.1 eV (*e.g.*, −0.07 eV for N^N = ampy and solvent = H_2O). The DFT calculated electronic and free energy changes of DFT reaction (10), corresponding to the net reaction of (2) for N^N = ampy, slowly decrease when considering the bipy, ampy, and en complexes, respectively, in agreement with a faster reaction for the en complexes, see energies in Table 3.

For DFT reaction (11), the conversion of formato into hydrido complexes (corresponding to the net reaction of (5) for

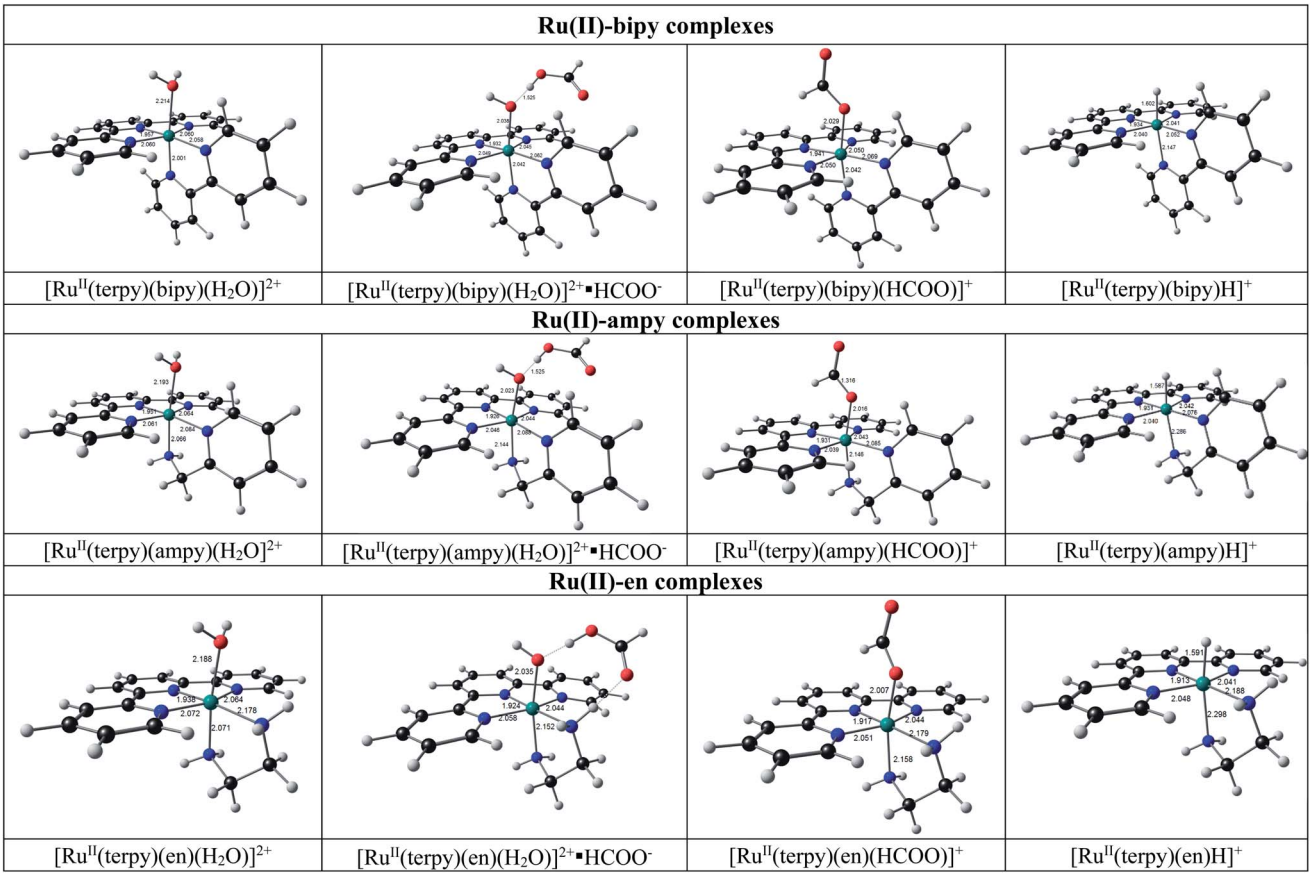

Fig. 12 Structures of complexes predicted for the conversion of $[Ru^{II}(terpy)(N^N)(H_2O)]^{2+}$ into $[Ru^{II}(terpy)(N^N)H]^+$ by DFT calculations. See Fig. S2† for the related $[Ru^{II}(terpy)(N^N)(EtOH)]^{2+}$ and $\{[Ru^{II}(terpy)(N^N)(EtOH)]^{2+}\cdot HCOO^-\}$ complexes. Colour scheme used for atoms (online version): Ru (green), O (red), C (black), N (blue), and H (white).

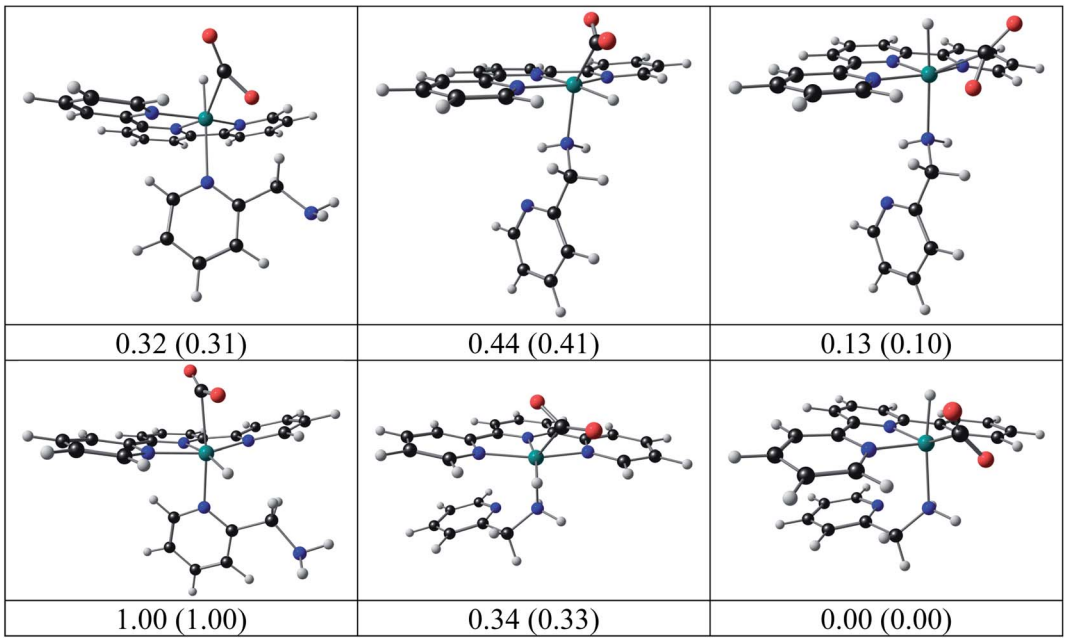

Fig. 13 Possible intermediates for reaction (5) calculated by DFT, relative electronic energy, with free energy in brackets (eV), indicated. Colour scheme used for atoms (online version): Ru (green), O (red), C (black), N (blue), and H (white).

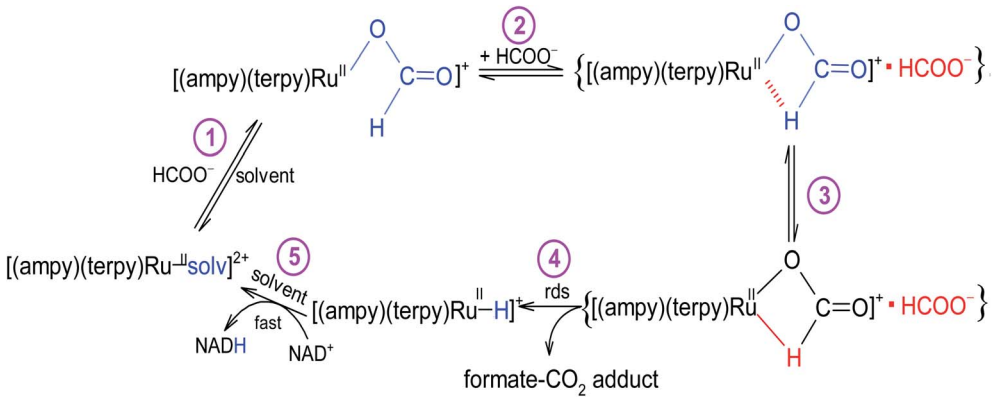

Scheme 1 The mechanism proposed for the NAD$^+$ coenzyme reduction in the presence of formate catalysed by a non-organometallic ruthenium(II) polypyridyl amine complex.

N^N = ampy), the calculated energy changes also slowly decrease when considering the bipy, ampy, and en complexes in agreement with a faster reaction for the en complexes, see energies in Table 3.

The structures of the hydrido complexes [Ru^{II}(terpy)(N^N)H]$^+$ are shown in Fig. 12. No experimental solid-state structure of a ruthenium(II)-terpy-hydrido complex containing a bidentate N^N ligand could be found in the literature; only ruthenium(II)-terpy-hydrido complexes containing two triphenylphosphine groups.[42,43] The [Ru^{II}(terpy)(ampy)H]$^+$ complex has the amine nitrogen *trans* to H, with the [Ru^{II}(terpy)(ampy)H]$^+$ complex with the amine nitrogen *cis* to the H more than 0.2 eV higher in both electronic and free energies. Some possible reaction intermediates were also identified for reaction (5) of the Ru-ampy complex (Fig. 13). The geometry of the intermediates differs by (i) the relative positions of H and CO_2 to the singly coordinated ampy, (ii) the coordination N of singly coordinated ampy (through N amine or N pyridyl), and (iii) the orientation of the uncoordinated pyridyl ring. The molecule with H and the amine nitrogen *trans* to H in the axial positions, CO_2 and the terpy N's in the equatorial positions, with one uncoordinated pyridyl ring, has the lowest energy. The aromatic pyridyl ring is not bonded to ruthenium, orientated near parallel to the terpy rings, and stabilized by π–π interactions between the aromatic rings. A similar uncoordinated pyridyl ring, also orientated near parallel to terpy rings, is observed for the solid-state structure of a ruthenium(II) polypyridyl complex [Ru(terpy)(proline)(PPh_3)],[44] though the distance between the rings was much larger in the latter.

DFT calculations identified the geometries and energies of the ruthenium reactants, products, and possible reaction

intermediates involved in the kinetic reactions measured in this study. The DFT calculated energies show that the solvent-formato exchange and the formato-hydrido conversion reactions have negative (favourable) energies to proceed spontaneously and that the reactions involving en-containing molecules, have the more negative (favourable) energies, followed by ampy-containing molecules, in agreement with a faster reaction for en-containing molecules and slower reactions for bipy-containing molecules.

Overall discussion

The newly studied ampy complex reacts 11–18 times slower than the en complex under the selected conditions. This results from displacing the ethylenediamine ligand by 2-(aminomethyl) pyridine and the π-back bonding effect of the pyridine ring. A similar effect was observed for the corresponding complex with 2,2′-bipyridine (bipy) as a N^N bidentate spectator ligand. The stronger π-back bonding effect of bipy decreased the reactivity of the Ru(II) complex by many orders of magnitude, such that the hydride transfer reaction to the NAD^+ coenzyme was extremely slow (see Fig. S1†). By way of comparison, the NAD^+ reduction reaction catalysed by $[Ru^{II}(terpy)(ampy)(H_2O/EtOH)]^{2+}$ completes within 21 h and is accompanied by an absorbance increase of *ca.* 1.3 at 340 nm (due to formation of NADH, Fig. 7b), whereas ΔA_{340} during the reaction catalysed by $[Ru^{II}(terpy)(bipy)(H_2O/EtOH)]^{2+}$ reaches a value of only 0.2 after *ca.* 42 h under the same experimental conditions (Fig. S1†).

The studied conversion of NAD^+ to NADH in the presence of formate starts with the anation of the $[Ru^{II}(terpy)(ampy)(H_2O/EtOH)]^{2+}$ complex (see Scheme 1), which leads to the generation of the $[Ru^{II}(terpy)(ampy)(HCOO)]^+$ complex (step 1). In the second step, the excess of $HCOO^-$ enables the formation of the outer-sphere ion-pair complex $\{[Ru^{II}(terpy)(ampy)(HCOO)]^+ \cdot HCOO^-\}$. Subsequently (step 3), the slow, formate-induced rearrangement of the formato complex (from an end-on to an O,H bonding mode of formate) occurs. The O,H-bonded format complex releases the formate-CO_2 adduct and forms the hydrido complex $[Ru^{II}(terpy)(ampy)H]^+$ in step 4. The latter complex donates the hydride anion to NAD^+ to form NADH in a non-rate determining step, and regenerates the $[Ru^{II}(terpy)(ampy)(H_2O/EtOH)]^{2+}$ complex (step 5). In this way, the catalyst is reformed, as shown in the overall reaction Scheme 1. Since the reduction of NAD^+ to NADH by $NaBH_4$ occurs on a much shorter time scale[24] than the decarboxylation reaction of the precursor $\{[Ru^{II}(terpy)(ampy)(HCOO)]^+ \cdot HCOO^-\}$, the release of a formate-CO_2 adduct is suggested to be the rate-determining step of the overall redox process, catalysed by the Ru(II)-ampy complex (see Scheme 1).

Author contributions

MCh performed the synthetic work and kinetic measurements. JC performed DFT calculations. AK and RvE developed the manuscript concept and accepted responsibility for the reported work. All authors contributed equally to writing the manuscript.

Conflicts of interest

There is no conflict of interest among the authors.

Acknowledgements

This project was supported financially by the National Science Center, Poland, Grant No. 2019/33/N/ST4/00700. J. Conradie has received support from the South African National Research Foundation (grant numbers 129270 and 132504). The High-Performance Computing facility of the UFS, the CHPC of South Africa (Grant No. CHEM0947), and the Norwegian Supercomputing Program (UNINETT Sigma2, Grant No. NN9684K) are acknowledged for computer time.

References

1 I. Pérez-Torres, V. Guarner-Lans and M. E. Rubio-Ruiz, *Int. J. Mol. Sci.*, 2017, **18**, 2098.
2 R. L. Reyes and K. Tanaka, *Kimika*, 2017, **28**, 32.
3 W. Xiao, R. S. Wang, D. E. Handy and J. Loscalzo, *Antioxid. Redox Signaling*, 2018, **28**, 251.
4 L. Chaiswing, W. H. St. Clair and D. K. St. Clair, *Antioxid. Redox Signaling*, 2018, **29**, 1237.
5 M. D. Forrest, *bioRxiv*, 2015, 019307.
6 B. Poljsak, *J. Clin. Exp. Oncol.*, 2016, **5**, 4.
7 S. M. Hong, S. W. Hwang, T. Wang, C. W. Park, Y. M. Ryu, J. H. Jung, J. H. Shin, S. Y. Kim, J. L. Lee, C. W. Kim, J. L. Lee, C. W. Kim, G. Yoon, K. H. Kim, S. J. Myung and K. Y. Choi, *Cancer Sci.*, 2019, **110**, 629.
8 A. F. Santidrian, A. Matsuno-Yagi, M. Ritland, B. B. Seo, S. E. LeBoeuf, L. J. Gay, T. Yagi and B. Felding-Habermann, *J. Clin. Invest.*, 2013, **123**, 1068.
9 I. Batinic-Haberle, A. Tovmasyan and I. Spasojevic, *Redox Biol.*, 2015, **5**, 43.
10 *Redox-active therapeutics. Oxidative stress in applied basic research and clinical practice*, ed. I. Batinic-Haberle, J. Reboucas and I. Spasojevic, Springer International Publishing, Switzerland, 2016.
11 L. Chaiswing, L. W. H. St. Clair and D. K. St. Clair, *Antioxid. Redox Signaling*, 2018, **29**, 1237.
12 C. Hegedűs, K. Kovács, Z. Polgár, Z. Regdon, É. Szabó, A. Robaszkiewicz, H. J. Forman, A. Martner and L. Virág, *Redox Biol.*, 2018, **16**, 59.
13 K. Wang, J. Jiang, Y. Lei, S. Zhou, Y. Wie and C. Huang, *Trends Biochem. Sci.*, 2019, **44**, 401.
14 A. Privat-Maldonado, A. Schmidt, A. Lin, K. D. Weltmann, K. Wende, A. Bogaerts and S. Bekeschus, *Oxid. Med. Cell. Longevity*, 2019, 9062098.
15 J. L. Quiles, C. Sánchez-González, L. Vera-Ramírez, F. Giampieri, M. D. Navarro-Hortal, J. Xiao, J. Llopis, M. Battino and A. Varela-López, *Antioxid. Redox Signaling*, 2020, **33**, 860.

16 A. M. Barbosa, J. F. Sarmento-Neto, J. E. R. Menezes Filho, I. C. G. Jesus, D. S. Souza, V. M. N. Vasconcelos, F. D. l. Gomes, A. Lara, J. S. S. Araújo, S. S. Mattos, C. M. L. Vasconcelos, S. Guatimosim, J. S. Cruz, I. Batinic-Haberle, D. A. M. Araújo, J. S. Rebouças and E. R. Gomes, *Oxid. Med. Cell. Longevity*, 2020, 4850697.
17 S. Betanzos-Lara, A. Habtemariam and P. J. Sadler, *J. Mex. Chem. Soc.*, 2013, **57**, 160.
18 J. J. Soldevilla-Barreda, I. Romero-Canelon, A. Habtemariam and P. J. Sadler, *Nat. Commun.*, 2015, **6**, 6582.
19 C. Imberti and P. J. Sadler, *Adv. Inorg. Chem.*, 2020, **75**, 3.
20 P. Zhang and P. J. Sadler, *J. Organomet. Chem.*, 2017, **839**, 5.
21 J. P. C. Coverdale, J. Song, G. J. Clarkson, J. Kasparkova, A. Habtemariam, V. Brabec, J. A. Wolny, V. Schüneman and P. J. Sadler, *Dalton Trans.*, 2018, **47**, 7178.
22 J. J. Soldevila-Barreda, P. C. A. Bruijnincx, A. Habtemariam, G. J. Clarkson, R. J. Deeth and P. J. Sadler, *Organometallics*, 2012, **31**, 5958.
23 M. J. Chow and W. H. Ang, in *Inorganic and Organometallic Transition Metal Complexes with Biological Molecules and Living Cells*, ed. K. K.-W. Lo, Academic Press, 2017, ch. 4, pp. 119–146.
24 M. Chrzanowska, A. Katafias and R. van Eldik, *Inorg. Chem.*, 2020, **59**, 14944.
25 M. Chrzanowska, A. Katafias, O. Impert, A. Kozakiewicz, A. Surdykowski, P. Brzozowska, A. Franke, A. Zahl, R. Puchta and R. van Eldik, *Dalton Trans.*, 2017, **46**, 10264.
26 M. Chrzanowska, A. Katafias, A. Kozakiewicz, R. Puchta and R. van Eldik, *J. Coord. Chem.*, 2018, **71**, 1761.
27 M. Chrzanowska, A. Katafias, A. Kozakiewicz and R. van Eldik, *Inorg. Chim. Acta*, 2020, **504**, 119449.
28 C. D. Hubbard, D. Chatterjee, M. Oszajca, J. Polaczek, O. Impert, M. Chrzanowska, A. Katafias, R. Puchta and R. van Eldik, *Dalton Trans.*, 2020, **49**, 4599.
29 E. van Lenthe, E. J. Baerends and J. G. Snijders, *J. Chem. Phys.*, 1993, **99**, 4597.
30 E. van Lenthe, E. J. Baerends and J. G. Snijders, *J. Chem. Phys.*, 1994, **101**, 9783.
31 E. van Lenthe, A. Ehlers and E. J. Baerends, *J. Chem. Phys.*, 1999, **110**, 8943.
32 N. C. Handy and A. J. Cohen, *Mol. Phys.*, 2001, **99**, 403.
33 C. T. Lee, W. T. Yang and R. G. Parr, *Phys. Rev. B: Condens. Matter Mater. Phys.*, 1988, **37**, 785.
34 S. Grimme, J. Antony, S. Ehrlich and H. Krieg, *J. Chem. Phys.*, 2010, **132**, 154104.
35 G. te Velde, F. M. Bickelhaupt, S. J. A. van Gisbergen, C. F. Guerra, E. J. Baerends, J. G. Snijders and T. Ziegler, *J. Comput. Chem.*, 2001, **22**, 931.
36 C. F. Guerra, J. G. Snijders, G. te Velde and E. J. Baerends, *Theor. Chem. Acc.*, 1998, **99**, 391.
37 S. Kern and R. van Eldik, *Inorg. Chem.*, 2012, **51**, 7340.
38 W.-H. Wang, S. Xu, Y. Manaka, Y. Suna, H. Kambayashi, J. T. Muckerman, E. Fujita and Y. Himeda, *ChemSusChem*, 2014, **7**, 1976.
39 X.-J. Yang, F. Drepper, B. Wu, W.-H. Sun, W. Haehnel and C. Janiak, *Dalton Trans.*, 2005, 256.
40 K. Qvortrup, C. J. McKenzie and A. D. Bond, *Acta Crystallogr., Sect. E: Struct. Rep. Online*, 2007, **63**, m1400.
41 N. Grover, N. Gupta, P. Singh and H. H. Thorp, *Inorg. Chem.*, 1992, **31**, 2014.
42 H. Konno, A. Kobayashi, K. Sakamoto, F. Fagalde, N. E. Katz, H. Saitoh and O. Ishitani, *Inorg. Chim. Acta*, 2000, **299**, 155.
43 A. Pramanik, N. Bag and A. Chakravorty, *J. Chem. Soc., Dalton Trans.*, 1992, 97.
44 P. Kumar, A. K. Singh, J. K. Saxena and D. S. Pandey, *J. Organomet. Chem.*, 2009, **694**, 3570.